Effects of hypochlorite exposure on the structure and electrochemical performance of ion exchange membranes in reverse electrodialysis

Ying Mei [a], Zhikan Yao [a], Lihui Ji [b], Patrick H. Toy [c], Chuyang Y. Tang [a,*]

[a] Department of Civil Engineering, The University of Hong Kong, Pokfulam Road, Hong Kong S.A.R., P.R. China

[b] School of Environmental Engineering, Harbin Institute of Technology, Harbin150090, P.R. China

[c] Department of Chemistry, The University of Hong Kong, Pokfulam Road, Hong Kong S.A.R., P.R. China

*Corresponding author address: HW6-19B Haking Wong Building, Department of Civil Engineering, the University of Hong Kong, Pokfulam, Hong Kong; Tel: (+852) 28591976; E-mail: tangc@hku.hk

Abstract

We performed chlorination experiments to understand the impact of hypochlorite exposure on both cation exchange membranes (CEMs) and anion exchange membranes (AEMs) regarding their properties and performance in a reverse electrodialysis (RED) stack. Changes in membrane morphology, surface elemental composition and chemical bounding suggested the chlorine incorporation in the form of C-Cl bonds and side-chain cleavage of $–SO_3^-$ or $–NR_3^+$ containing molecular fractions. These observations were further supported by observed increases in hydrophobicity and decreases in fixed charged groups of the membranes, respectively. Compared to CEMs, AEMs were less chlorine resistant such that the development of more extensive cracks in the membrane structure further increased water content and dramatically decreased membrane conductivity. The performance of both chlorinated CEMs and AEMs were tested in an RED stack and the results showed the reduced RED power density was largely attributed to the deteriorated electrical properties of AEMs.

Keywords: Reverse electrodialysis (RED); Salinity gradient power (SGP); Ion exchange membrane; Sodium hypochlorite; Chlorination mechanism;

1. Introduction

When 1 m^3 of freshwater is mixed with seawater, a Gibbs free energy of approximately 0.8 kWh is released [1-4]. This energy, arising from the salinity difference between the two aqueous solutions, is commonly known as osmotic energy or salinity gradient power (SGP) and is considered as an emerging form of renewable energy. One mainstream technology to harvest SGP is reverse electrodialysis (RED), in which ionic current formed under the concentration difference driving force is converted into electricity [2, 3, 5]. Recently, an RED pilot has demonstrated a power production of 330 W utilizing real saline solutions from saltworks [6]. With further development of membranes of high power density as well as novel RED processes [], SGP production can be potentially competitive against alternative renewable energy sources.

Membrane fouling is a serious issue in RED. The use of seawater, river water, and/or treated wastewater in RED processes can cause colloidal fouling, organic fouling, and bio-fouling, resulting in a significant reduction in achievable power density [7-9]. Several anti-fouling strategies have been reported in the context of RED, including operational measures (e.g., feedwater reversal and air sparging [10]), improved water feed channels to achieve more uniform flow distribution [11], and membrane surface modification [12]. In addition, chemical cleaning can play an important role in restoring membrane performance. One of the most commonly used cleaning agents is hypochlorite. Although its use in RED has not been reported yet, hypochlorite has been widely used in removing biofouling and organic fouling in membrane bioreactors [13] and membrane filtration processes [14-16]. The use of hypochlorite in cleaning electrodialysis (ED) membranes has also recently been studied [17]. Nevertheless, frequent cleaning of ion exchange membranes (IEMs) could alter the chemical structure of the membranes as well as adversely affect their electrochemical performance [17]. Studies in the context of ED have been focused on the membrane aging effect under chlorine exposure and the development of chlorine resistant IEMs [{Pretz, 1999 #2273}]. The lack of detailed studies on hypochlorite cleaning in RED calls for systematic investigations on the interaction mechanism of hypochlorite and IEMs and therefore the RED power performance.

In this study, we investigated the effects of sodium hypochlorite exposure on the chemical structure and electrochemical properties of IEMs and their performance in RED. Our study may provide important insights into the underlying mechanisms of IEM chlorination.

2.Materials and Methods

2.1 Chemicals and Materials

The commercial cation exchange membrane (CEM) and anion exchange membrane (AEM) used in the current study were Selemion^{TM} CMV® and AMV® (AGC Engineering CO., LTD, Japan). Both CMV and AMV were homogeneous membranes. The molecular structures of these membranes are shown in Fig. 1. According to the manufacturer, CMV is made by cross-linking polystyrene (PS) and divinylbenzene (DVB) on a substrate fabric of polyvinyl chloride

(PVC) cloth, followed by sulfonation in concentrated sulfuric acid. AMV is made by crosslinking PS, DVB and chloromethylstyrene (CMS) on a PVC cloth, followed by quaternization. Proprietary additives are also used during the membrane fabrication process. All the membranes were pre-soaked in deionized (DI) water for at least 24 h to remove any impurities from the manufacturing processes and stored in DI water at 4 °C.

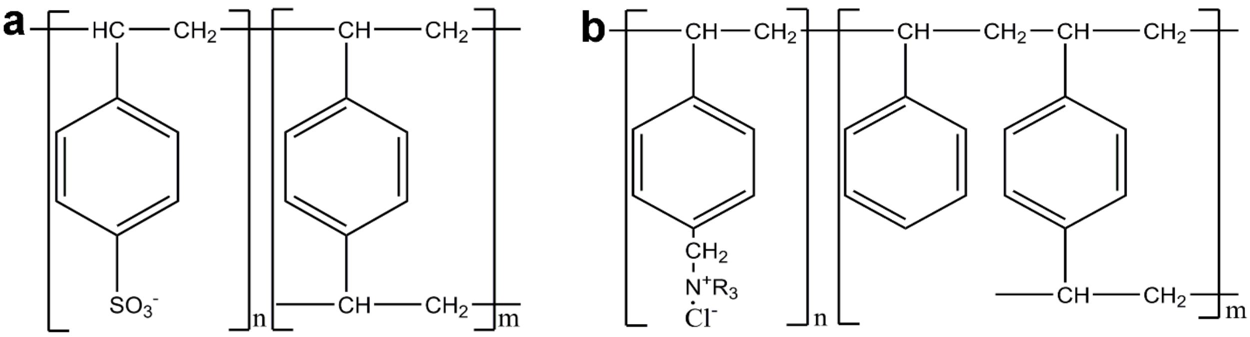

Fig. 1. Molecular structures of (a) virgin CEM with sulfonate functional group and (b) virgin AEM with quaternary ammonium functional group.

All the chemicals used in this study were of analytical grade and were used as received. Sodium hypochlorite soaking solutions were prepared by diluting commercial concentrated 5% NaClO solution (Unichem Laboratories Ltd., Asia) with DI water. The total active chlorine concentration was determined through the standard iodometric titration method using sodium thiosulfate, and recorded as ppm of Cl equivalent [18].

2.2 Membrane chlorination protocol

The chlorination procedures were adapted from Tang and coworkers [15, 19, 20]. Before each chlorination test, a membrane coupon with an area of 15×15 cm^2 was dried with filter paper to remove access water on the membrane surface, and then pre-washed for about 1 min in a NaClO solution before being immersed into the chlorination solution. Both the pre-washing solution and chlorination solution had identical water chemistry (100, 1000 or 5000 ppm active chlorine at pH 7). Chlorination was performed in 1 L sealed bottle that was covered with aluminum foil to prevent chlorine degradation. The bottle was constantly shaken at room temperature (~ 25 °C) over the entire chlorination duration of 50 h. Both chlorine concentration and pH were monitored throughout the test, and NaClO was replenished accordingly to ensure that active chlorine concentration was at least 80 % of its initial value [20]. The chlorinated membrane coupon was rinsed with DI water thoroughly until the remaining chlorine concentration in the rinsed water was undetectable, avoiding any further reaction. Membrane electrochemical properties and swelling degree were examined on wet samples immediately after chlorination, while other chemical characterization (e.g., SEM, XPS, FTIR-ATR, contact angle) were performed on vacuum-dried samples.

2.3 Membrane characterization

2.3.1 Membrane surface morphology and chemistry characterization

To obtain membrane surface and cross section morphology information, a field-emission scanning electron microscope analysis (FE-SEM, Hitachi S-4800, Japan) was performed on dry membrane samples sputter-coated with a homogeneous layer of gold (SCD 005, BAL-TEC, NYC). The acceleration voltage of SEM micrographs was set at 5 kV. X-ray photoelectron spectroscopy (XPS) was employed to obtain elemental composition of the surface layer (top 1-5 nm thickness). XPS analysis was operated on PHI 5000C ESCA System (Physical electronics, Inc., U.S.) for 3 times per sample over a range of 0-1200 eV. Results were fitted using XPS Peak 4.1 software with background type of Linear. The information regarding membrane bonding chemistry was obtained by attenuated total reflection-fourier transform infrared (ATR-FTIR) (Spectrometer 100, PerkinElmer Inc., U.S.). Each spectrum was averaged from 16 scans over a wave number range of 4000-500 cm^{-1}. Water contact angle measurements were also conducted using a contact angle goniometer (Powereach, China). Each DI water droplet of 8 μL was dripped on the membrane surface and stabilized for 10 s before measurement. At least 5 parallel experiments were performed at different locations and the average value was reported.

2.3.2 Membrane ion exchange capacity (IEC), swelling degree (SD) and fixed charge density (FCD)

Most of the membrane properties and electrical performance are related to the type and concentration of fixed ionic groups in the membrane matrix and that of surrounding electrolytes. The transport of counter-ions (e.g., cations in terms of CEMs and anions in terms of AEMs) is realized by both of the counter-ions in electrical equilibrium with fixed charges and the free counter-ions in excess to the membrane charge [21, 22]. The amount of counter-ions native to membrane inner surface is directly determined by the amount of fixed ionic charges attached to the membrane backbone, which can be evaluated as the IEC [22, 23]. Furthermore, the concentration and mobility of free counter-ions in the membrane matrix are influenced by the water uptake and swelling degree of membrane samples [24].

IEC can be evaluated as the milli-equivalents of functional groups per gram of dry membrane [24]. In this study, IEC was determined by titration of the counter-ions of the specific membranes (e.g. H^+ for CMV and Cl^- for AMV) [23, 24]. For CMV, membrane samples with an area of 3×3 cm^2 were immersed in an excess amount of 1 M HCl over night at room temperature, with the soaking solution was refreshed at least two times to convert the membranes into H^+ form. Afterwards, immersed membranes were thoroughly rinsed with DI water to remove the excess acid. Then the protons were exchanged into solution for titration by immersing the membranes in 2 M NaCl solution for 24 h (the soaking solution was refreshed two times to complete ion exchange). After collecting all the NaCl solutions, the acid titration was performed with 0.001 M NaOH solution. The mass of protons was directly related to the fixed charges in the ion exchange membranes. Finally, membrane samples were dried at 60 ºC overnight to measure their dry mass weight. Similarly, AMV samples were firstly immersed in an excess amount of 3 M NaCl (the solutions were changed for at least two times) overnight to turn the membranes into the Cl^- form. Afterwards, membrane samples were rinsed in DI water to eliminate access Cl^-, and subsequently immersed in 3 M $NaNO_3$ for 24 h (the solutions were replaced two times). The $NaNO_3$ solutions were combined together and the corresponding chloride concentration was determined by ion exchange chromatography. The mass of chloride was used to determine the IEC of AMV.

The water-uptake of an ion exchange membrane was evaluated in terms of swelling degree (SD), i.e., the ratio of the amounts of absorbed water to dry weight of the corresponding membrane samples (Eq. (1)):

$$SD = \frac{m_{wet} - m_{dry}}{m_{dry}} \times 100\% \tag{1}$$

where m is the measured weight of membrane samples, the subscribe *wet* and *dry* indicates membrane state before and after drying. Before measuring SD values, membrane samples were pre-soaked in DI water for at least 48 h. Subsequently, they were wiped and pressed dried with filter paper. After measuring their wet weight (m_{wet}), the membrane samples were dried in an oven at 40 °C overnight until a constant dry weight (m_{dry}) was obtained.

Fixed charge density (FCD) represents the charged groups concentration in terms of the water phase. It can be calculated from dividing IEC by SD as Eq. (2):

$$FCD = \frac{IEC}{SD} \tag{2}$$

2.3.2 Membrane permselectivity

The ability of ion exchange membrane to discriminate between counter-ions (i.e., cations for CEMs and anions for AEMs) and co-ions (i.e., anions for CEMs and cations for AEMs) can be quantified by permselectivity. Membrane permselectivity can be influenced by fixed charge groups density as the electrostatic exclusion of co-ions, as well as the water volume fraction due to the resulting dimensional structure (e.g., large water volume fraction denotes loose mechanical structure and lower cross-linking level) [23].

The apparent permselectivity (α) can be measured from the ratio of electrical diffusion potential (E_{meas}) over the membrane sample separating solutions of different salinity and the corresponding theoretical value (E_{theo}) based on Nernst equation assuming a permselectivity of unity [24]:

$$\alpha = \frac{E_{meas}}{E_{theo}} \times 100\% \tag{3}$$

As shown in the Fig. 2a, a characterization setup with two cells (each of 64 mL) was applied to measure the membrane permselectivity. A circular disk of membrane sample with an effective area of 3.14 cm^2 was soaked in a 0.02 M NaCl solution overnight before being placed between the two cells. Two Ag/AgCl reference electrodes (CHI111, CH Instruments Inc.), located in Habber Luggin Capillaries filled with 3 M KCl, were applied for measuring the voltage across the membrane. A concentrated solution of 0.6 M NaCl and a diluted solution of 0.02 M NaCl were used in a high salinity (HS) and low salinity (LS) compartments, respectively. Each measurement was carried out for 5 min to obtain a steady state voltage reading.

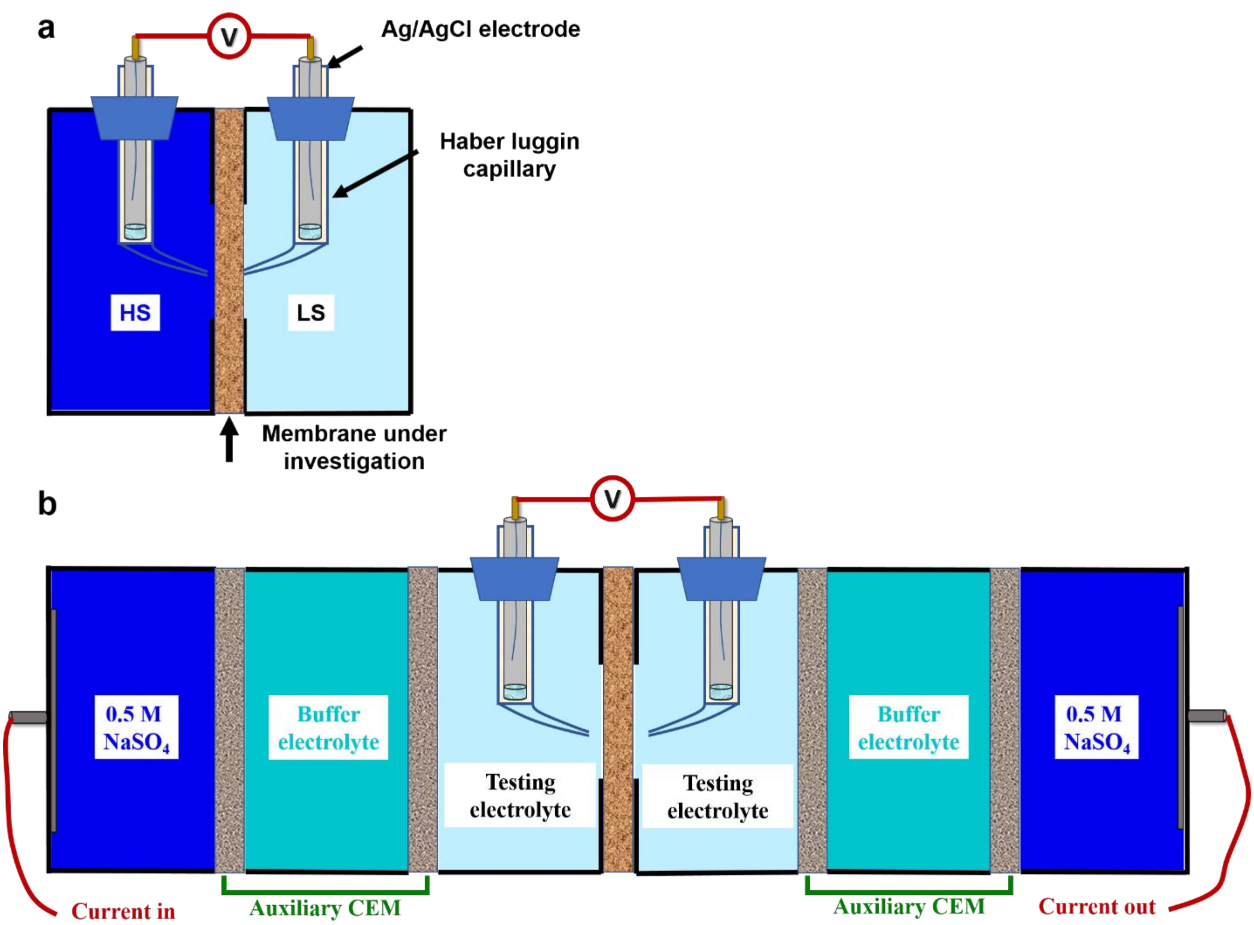

Fig. 2. Schematic diagram of an experimental setup for (a) membrane permselectivity characterization over a concentration gradient of HS and LS, (b) membrane resistance characterization in salt solution of specific concentrations.

2.3.4 Membrane resistance

Membrane resistance was measured in solutions of constant concentration of 0.6 M or 0.1 M NaCl. The testing setup, in a six-compartment configuration (Fig. 2b), was adapted from the literatures [21, 24, 25]. A membrane sample of interest (circular disk of an active area of 3.14 cm^2) was installed in the middle of the reactor. Additional auxiliary CEMs (4 pieces, each of 50.24 cm^2) were used to separate the testing solution, buffer solution, and electrode solution in different compartments. The buffer solutions, which had identical composition to the testing solutions, were adopted to avoid the leakage of redox reaction products in the end compartments and to reduce the concentration fluctuation in the testing compartments. Platinum coated titanium electrodes (Magneto special anodes B.V. China) were situated in the two end compartments which were filled with 0.5 M Na_2SO_4 to avoid the formation of chlorine. All the solutions used in the reactor were circulated during operation at a constant flow rate of 120 mL/min. During measurement, chronopotentiometry using direct current (DC) was performed with a series of current steps (e.g., 1-3 mA with an interval of 0.5 mA for 180 s) injected through platinum electrodes. The corresponding voltage drop across the testing membrane was continuously recorded with Ag/AgCl reference electrodes inserted Haber-Luggin capillaries. The gross area resistance ($\Omega \cdot cm^2$) was calculated as the slope of the polarization curve (current density on the x axis and voltage output on the y axis). The net membrane resistance was obtained by deducting the resistance of testing electrolytes, obtained from parallel blank test without the installation of the membrane, from the gross value [26].

2.4 RED performance testing

To investigate the impacts of chlorination on RED performance, the chlorinated membranes and virgin membranes were tested in a lab-scale RED stack (Fig. 3) that was similar to what has been previously reported [27-30]. The stack consisted of five pairs of IEMs, each composed of one CEM, one AEM with spacers and gaskets in between for defining the feed flow channels between the membranes. The electrodes used in the stack were made of titanium meshes coated with Ru/Ir metal oxide (effective area of 10×10 cm^2). Synthetic feed solutions of 0.6 M and 0.02 M NaCl were used as HS solution and LS solution, respectively. Both HS and LS were fed to the stack at a constant rate of 70 mL/min. Meanwhile, an electrolyte containing 0.3 M NaCl, 0.05 M $K_4Fe(CN)_6$ and 0.05 M $K_3Fe(CN)_6$ was circulated through the electrode compartments at a flow rate of 60 mL/min [27]. Chronopotentiometry was conducted on the RED stack with a series of current steps (e.g., 4 A/m^2-23 A/m^2 with a current step of ~ 4 A/m^2). The RED power density was determined as the product of the current density and the output voltage [31].

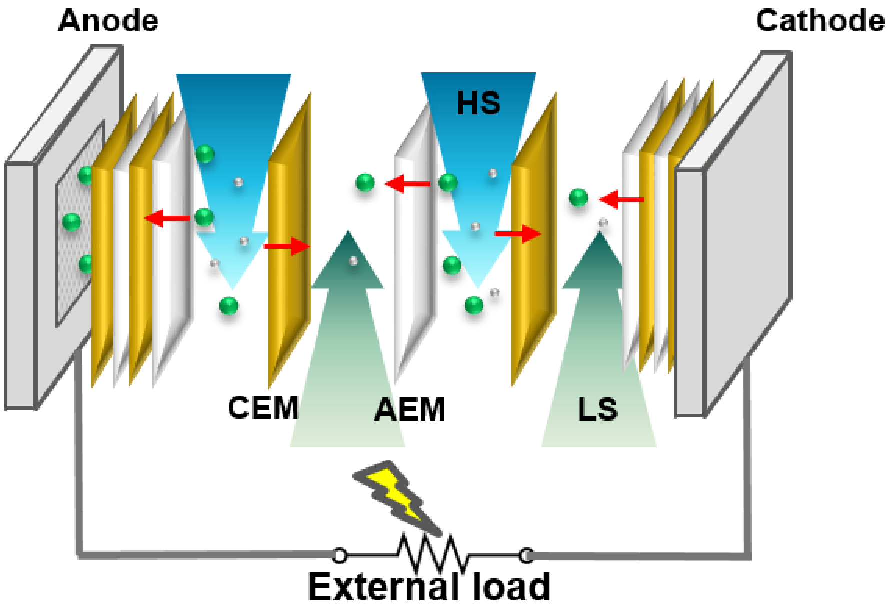

Fig. 3. Schematic diagram of RED performance evaluation system [30].

3. Results and Discussion

3.1 Changes in membrane morphology and chemistry due to chlorination

3.1.1 Changes in membrane morphology

Fig. 4 shows the surface and cross-section SEMs of virgin and chlorinated CEMs. The virgin CEM exhibited a flat, smooth and homogeneous surface with the exception of a few pinholes or local defects (Fig. 4a). Its cross-section (inset in Fig. 4e) showed an interpenetrating network of ion exchange polymer supported by the PVC substrate, consistent with the information provided by the manufacturer. Upon exposure to 100 – 5000 ppm hypochlorite solution for 50 h, the membrane surface morphology was significantly altered. At lower hypochlorite concentrations (100 and 1000 ppm), localized cracks appeared (Fig. 4b and 4c). Further increase of hypochlorite concentration to 5000 ppm resulted in the extensive development of cracks throughout the membrane, which was also accompanied with severe surface erosion (Fig. 4d). The corresponding cross-section image (inset of Fig. 4f) shows that the polymer coverage above the cloth became thinner, and the texture of PVC cloth can be clearly observed. The cross-sectional image at higher magnification (Fig. 4f) revealed the formation of numerous particles whose diameter was on the order of 100 - 200 nm, possibly attributed to the residue of polymer corrosion. Similar damages were also observed for the AEM upon chlorination (Fig. 5). However, compared to the CEM, the AEM developed more extensive cracks at higher hypochlorite concentrations (1000 and 5000 ppm), indicating that the AEM was more sensitive to hypochlorite exposure.

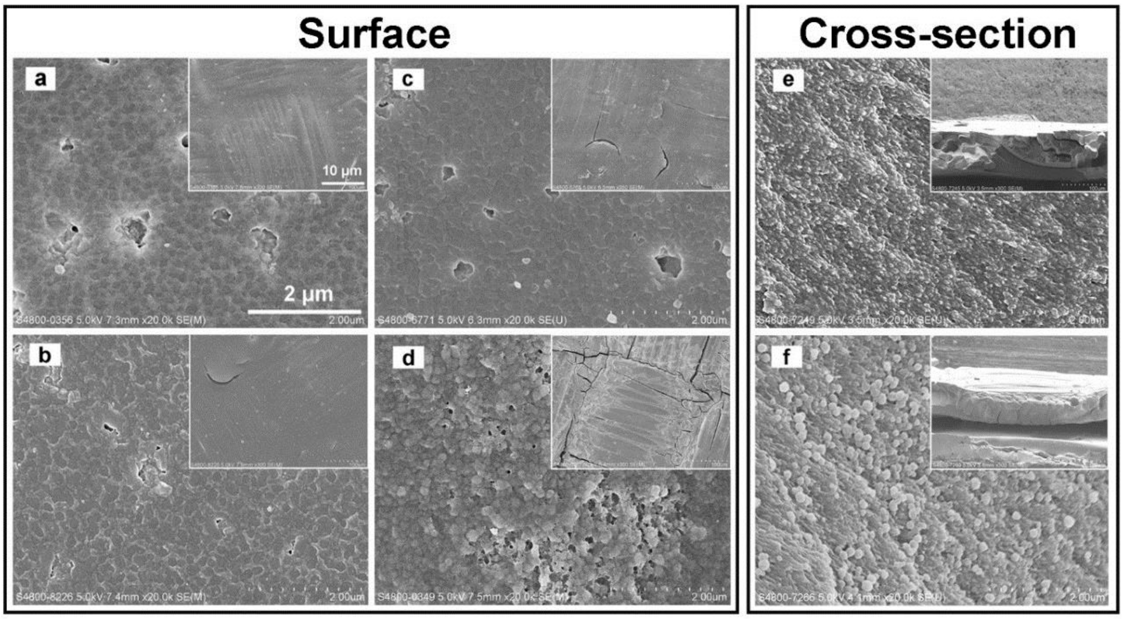

Fig. 4. SEM images of membrane surface (a-d) and cross-section (e-f): virgin CEM (a, e) and CEM chlorinated in 100 ppm (b), 1000 ppm (c), and 5000 ppm (d, f) for 50 h at pH 7.

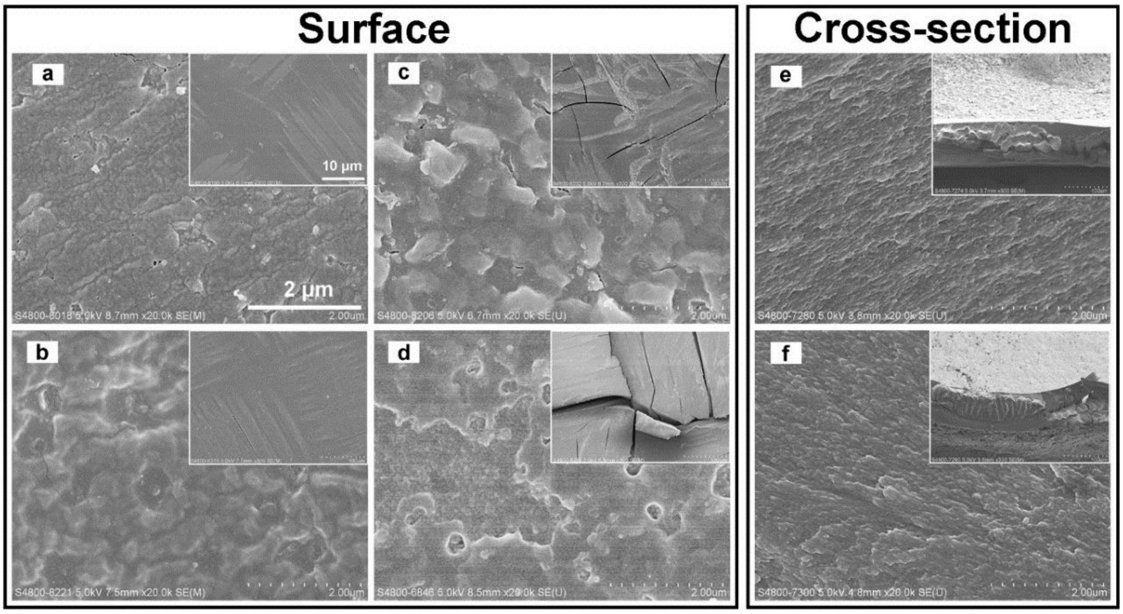

Fig. 5. SEM images of membrane surface (a-d) and cross-section (e-f): virgin AEM (a, e) and AEM chlorinated in 100 ppm (b), 1000 ppm (c), and 5000 ppm (d, f) for 50 h at pH 7.

3.1.2 Changes in elemental composition and chemical bonding

Table 1 presents the surface elemental composition of both virgin and chlorinated membranes. Despite the fact that the chemical structure of the CEM contained no nitrogen (Fig. 1a), XPS measurements showed 1.4 % N. According to the manufacturer, the nitrogen content in the CEM can be attributed to the residual –CN containing additives used in the membrane fabrication process. Both CEM and AEM virgin membranes contained small amount of chlorine due to the presence of the PVC fabric. Upon hypochlorite exposure, the amount of chlorine incorporated into both CEMs and AEMs increased at greater active chlorine concentrations. For the CEM, this increase in chlorine content was accompanied by a decrease of sulfur and oxygen contents, although the change in the Cl % was far more significant compared to those for S % and O %. These observations suggest the simultaneous incorporation of Cl into the chlorinated CEM and the cleavage of $–SO_3$ containing molecular fractions from the polymer chains. Compared to the CEM, less additional chlorine was incorporated into the AEM (e.g., ~ 3 % increase for AEM vs. ~ 6.7 % increase in CEM at 5000 ppm hypochlorite concentration). The minor decrease of nitrogen content in the AEM may be caused by the loss of its quaternary ammonium functional groups during chlorination.

Table 1. Surface elemental composition of virgin and chlorinated ion exchange membranes upon hypochlorite exposure.

Membrane type	Chlorine concentration (ppm) [a]	C (%)	O (%)	S (%)	N (%)	Cl (%)
CEM [c]	0	75.4±1.6	19.4±2.0	2.27±0.0	1.38±1.1	1.40±0.7
CEM [c]	100	74.8±2	18.6±2.3	1.8±0.2	2.6±0.5	1.9±0.1
CEM [c]	1000	75.2±0.9	18.1±1.7	1.7±0.1	1.5±1.4	3.5±0.4
CEM [c]	5000	74.4±3.6	16.2±0.9	1.3±0.2	N.D. [b]	8.1±3.1
AEM [d]	0	75.0±3.5	20.3±4.1	N.D. [b]	2.5±0.7	2.1±0.1
AEM [d]	100	75.7±4.9	20±5.8	N.D. [b]	2.1±0.3	2.2±0.7
AEM [d]	1000	75.8±0.2	18.8±0.5	N.D. [b]	2.2±0.5	3.1±0.1
AEM [d]	5000	74.9±0.9	18.2±2.5	N.D. [b]	1.6±0.7	5.1±1.3

Notes:

a. Chlorination was performed soaking the membranes in sodium hypochlorite solutions. The solution pH was 7 and the soaking duration was 50 h.

b. The particular element was below the detection limit. N.D. stands for not detected.

c. The CEM used in this study is Selemion™ CMV®

d. The AEM used in this study is Selemion™ AMV®

Fig. 6 shows the high resolution XPS spectra for the C 1s peak for the virgin and chlorinated membranes (5000 ppm × 50 h, pH 7). The shift in the binding energy relative to C-C (~ 285 eV) indicates the chemical bonding environment of the carbon element, with a higher binding energy shift δ_{BE} indicating a more highly oxidized state. For the CEM (Fig. 6a), the carbon peak was deconvoluted into C-C, C-S (δ_{BE} = 1.1 eV), C-Cl (δ_{BE} = 1.6 eV), and C=O (δ_{BE} = 3.3

eV) [32, 33]. The apparent increased in C-Cl peak and the decrease in C-C peak upon chlorination suggests the formation of additional C-Cl bond with breaking of C-C bond (e.g., by possible chlorine attachment to the benzene ring [34]). The AEM shows a similar increase in the C-Cl bonds. This was accompanied with a reduction of the C-N peak (δ_{BE} = 0.4 eV [33]), suggesting a possible detachment of ammonium functional groups from the membrane.

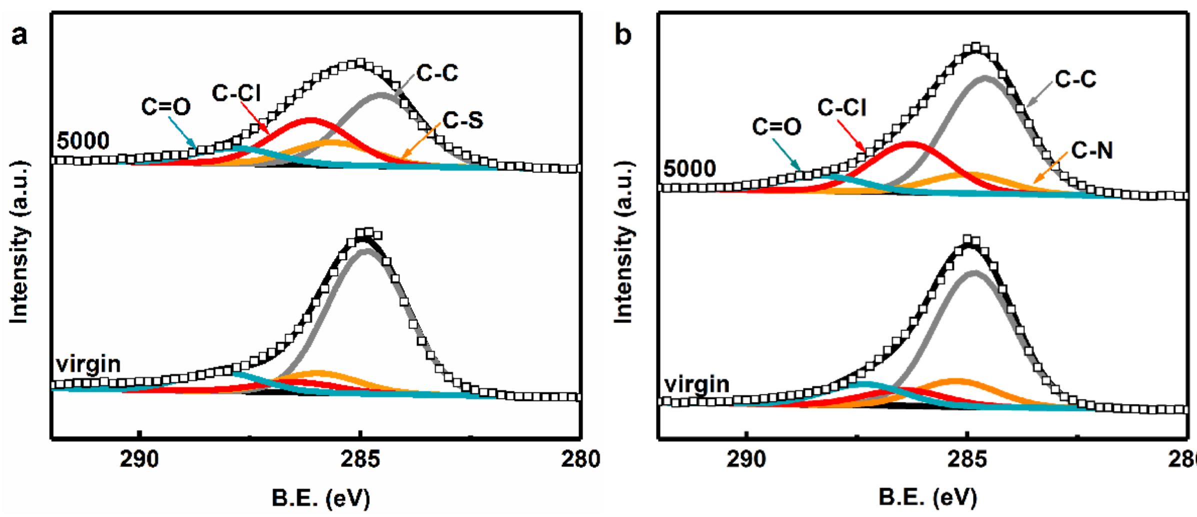

Fig. 6. High resolution XPS spectra and deconvoluted peak assignments of C 1s spectra for (a) virgin CEM and chlorinated CEM (5000 ppm × 50 h, pH 7), (b) virgin AEM and chlorinated AEM (5000 ppm × 50 h, pH 7). The binding energy shift of C-N, C-S, C-Cl, C=O were 0.4 eV, 1.1 eV, 1.6 eV, 3.3 eV, respectively.

Changes in chemical bonding and functional groups were characterized by ATR-FTIR over a wavenumber range of 4000-500 cm^{-1} (Fig. 7). The FTIR peak assignments and possible chlorination mechanisms are summarized in Table 2. The virgin CEM (Fig. 7a) presented a typical FTIR spectrum that is characteristic to membranes made from PS and DVB on a PVC cloth [17]. In the high frequency region (4000-2000 cm^{-1}), the broad band around 3700-3000 cm^{-1} (assigned to O-H vibration [35]) decreased upon chlorination. This can be attributed to a reduction of bound water, which is consistent with the increased contact angle of the membrane (Section 3.2.1). The absorption peak at 2850 cm^{-1}, corresponding to aliphatic C-H stretching vibration, disappeared after exposure to 5000 ppm hypochlorite, possibly due to the attack of membrane skeleton by chlorine. The weakening of band at 1640 cm^{-1}, assigned to aromatic ring breathing mode [17], may suggest the possible detachment of aromatic rings (e.g., -$C_6H_5SO_3^-$ side chain) and/or their attack by chlorine. These mechanisms are supported by XPS results showing reduced S % and O % (Table 1) and enhanced C-Cl peak (Fig. 6a). In addition, the reduced intensities for the peaks associated with the sulfonate groups (i.e., 1171 cm^{-1}, 1123 cm^{-1}, 1035 cm^{-1}, 1002 cm^{-1} for S-O, S=O and S-phenyl) may further support the mechanism of -$C_6H_5SO_3^-$ side chain cleavage.

Table 2. Summary of the peak assignments and possible chlorination mechanisms.

Origin of the peaks	Wavenumber (cm^{-1})	Peak assignments	Changes upon chlorination
Bound water	3430 and 3380	O-H bending vibration [36]	Weakened
Aliphatic chain	2850	Aliphatic C-H stretching [17]	Disappeared
PS-DVB material	3025, 704	Aromatic C-H stretching [37]	Disappeared
	1640, 1475	Aromatic ring breathing mode [17]	Weakened
	1980	C=C symmetric stretch [37]	No obvious change
Sulfonate	1175, 1125, 1035, 1007	S-O, S=O, S-phenyl [37, 38]	Weakened
Quaternary ammonium	1200-1250	C-N [17, 36]	No obvious change, possibly due to peak overlapping
Carbonyl group	1700	C=O [39, 40]	Only appeared on AEM
PVC cloth	2920	CH_2 asymmetric stretching band [17, 36]	Weakened
	1427	CH_2 bending deformation [41]	No obvious change
	1250	C-H stretching when the carbon was bonded to a chlorine atom [42]	No obvious change
	604	C-Cl [42]	Only strengthened on AEM

Similar to the CEM membrane, the AEM membrane (Fig. 7b) had a reduced intensity in the peak around 3380 cm^{-1} (O-H stretching) after chlorination. The disappearance of the aromatic C-H stretching band at 3025 cm^{-1} and 704 cm^{-1} and a reduction of intensity of aromatic ring breathing mode at around 1475 cm^{-1} suggest the possible attack of the aromatic ring of the PS-DVB material by chlorine. Meanwhile, the increased absorption intensity at 604 cm^{-1} may originate from the formation of new C-Cl bond. The characteristic absorption peaks for the quaternary ammonium groups were located at wave numbers of 1200-1250 cm^{-1} corresponded to the C-N stretching vibrations [17]. However, the bands overlapping around this frequency range make it difficult to distinguish between them. Furthermore, a new peak appeared at 1700 cm^{-1} that can be attributed to the band vibration of carbonyl groups [43].

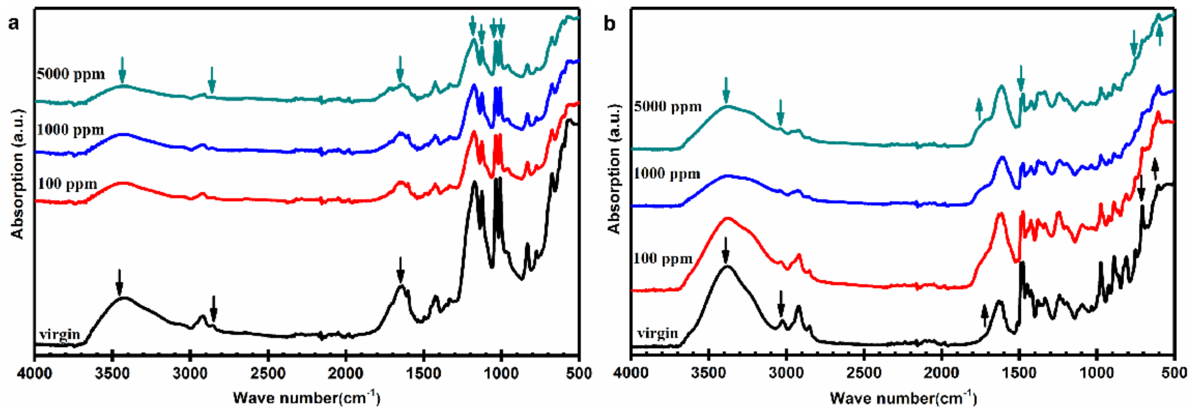

Fig. 7. ATR-FTIR spectra of (a) CEM and (b) AEM chlorinated in 0 ppm, 100 ppm, 1000 ppm and 5000 ppm at pH 7 for 50 h.

3.2 Changes in membrane properties due to chlorination

3.2.1 Changes in hydrophilicity, IEC, SD, FCD, and permselectivity

Hydrophobicity of membrane samples, indicating the difficulty in wetting a membrane surface [19], were evaluated by contact angle measurement (Fig. 8a). Both CEMs and AEMs became more hydrophobic after treatment with hypochlorite solutions of higher concentrations. These observations agree well with the past publications that report that the incorporation of chlorine into a membrane hinders its wetting and leads to an increase in hydrophobicity [15, 44, 45]

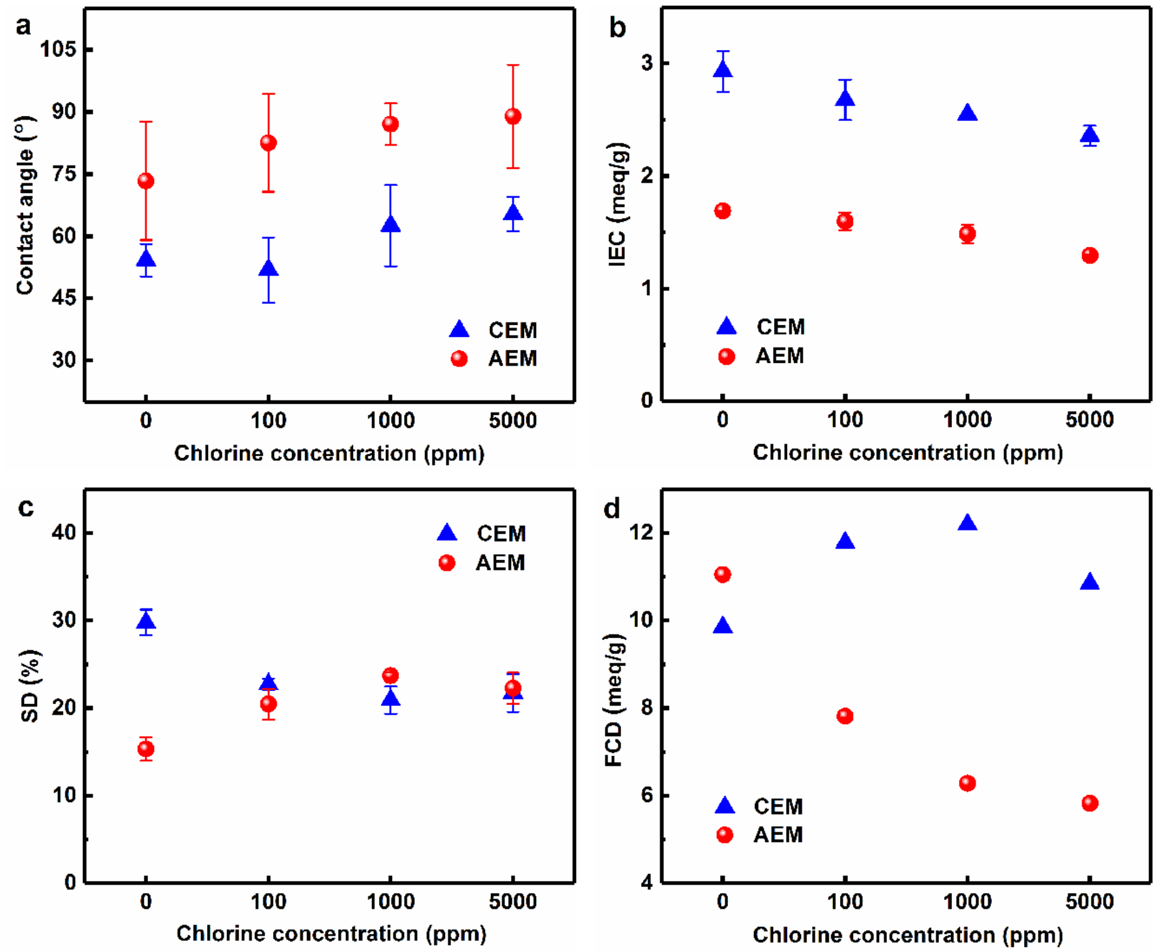

Fig. 8. Contact angle (degree) (a), ion exchange capacity (IEC) (b), swelling degree (SD) (c) and fixed charge density (FCD) (d) of IEMs chlorinated in 0 ppm, 100 ppm, 1000 ppm and 5000 ppm at pH 7 for 50 h.

Fig. 8b shows that the IEC of both CEM and AEM decreased as the total chlorine content increases, indicating a reduction of the fixed charge density of the membrane polymer upon chlorination. This observation is consistent with the proposed mechanism of chain cleavage of $–SO_3^-$ or $–NR_3^+$ containing fractions from membrane matrix (Section 3.1.2).

The water uptake of the CEM membrane, reflected by its swelling degree, decreased slightly after chlorination (Fig. 8c). The decreased SD can be attributed to the increased hydrophobicity (Fig. 8a), which is further consistent with the decreased bond water reflected by ATR FT-IR spectra (Fig. 7a). Interestingly, the AEM membrane shows an opposite trend of increased SD at higher hypochlorite concentrations. Compared to CEM, the AEM membrane developed more extensive cracks, which can allow for greater penetration of bulk water into the membrane structure. The dominance of the effect of membrane structural damage over the effect of hydrophobicity may explain the increased water uptake by the AEM membrane. The values of FCD can be defined as the ratio of IEC over SD. The CEM membrane had a relative constant FCD value over 0-5000 ppm hypochlorite concentration. In contrast, the AEM membrane experienced a dramatic reduction of FCD from 11 to 5.8 meq/g, due to the simultaneous decreased IEC and increased water content.

Greater permselectivity denotes the increased ability of an ion exchange membrane to discriminate between counter-ions and co-ions. In the current study, the permselectivity of the CEM and AEM mirrored the respective trends of FCD (Fig. 9). In particular, a dramatic loss of permselectivity of the AEM membrane occurred when the chlorine concentration was increased to 5000 ppm. This deterioration in permselectivity can be explained by the loss of charged functional groups combined with the severe damages to the membrane physical structure (e.g., cracks).

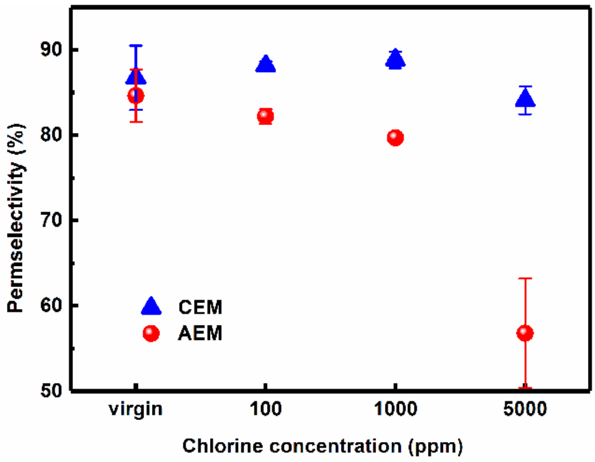

Fig. 9. Permselectivity of IEMs chlorinated in 0 ppm, 100 ppm, 1000 ppm and 5000 ppm at pH 7 for 50 h.

3.2.2 Changes in membrane resistance

The area resistance of both the CEM and AEM were evaluated in an electrolyte solution of 0.6 M NaCl (Fig. 10a). The value for the CEM was relatively constant even under severe chlorination conditions. In contrast, the electrical resistance of the AEM was more than doubled after exposure to 5000 ppm hypochlorite. Such an increase in the electrical resistance can be explained by the extensive cracks developed in addition to the chlorine attack to the quaternary ammonium groups in the AEM under severe chlorination (Fig. 5d). The cracks in the membrane could hinder the transport of counter ions within the ion exchange membrane matrix. To confirm our hypothesis, we further tested both virgin and chlorinated AEM membranes in a less concentrated electrolyte solution containing 0.1 M NaCl (Fig. 10b). For the virgin membrane that had an intact physical structure, its electrical resistance in 0.1 M NaCl was comparable to that measured in 0.6 M NaCl. In contrast, the physically damaged membranes (chlorinated at 1000 and 5000 ppm hypochlorite) showed a dramatic increase in electrical resistance when a lower concentration electrolyte solution was used. The filling of the cracks by a less concentrated electrolyte solution further suppresses the transport of counter-ions through the aqueous phase occupying the cracks, which enforces the ions to transport through a more tortuous route in the membrane matrix.

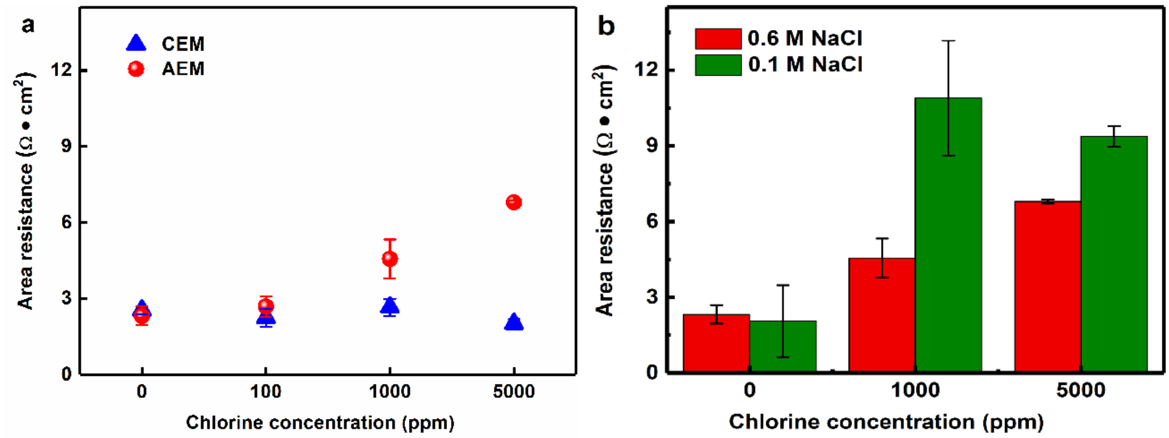

Fig. 10. Ionic resistances of IEMs tested in 0.6 M NaCl (a), AEMs tested in 0.6 M NaCl and 0.1 M NaCl (b). Chlorination conditions: 0 ppm, 100 ppm, 1000 ppm and 5000 ppm at pH 7 for 50 h.

3.3 Changes in the performance of an RED stack due to chlorination

To explore the effects of chlorinated IEMs on RED performance, voltage (Fig. 11a) and power output (Fig. 11b) of an RED stack using virgin and/or chlorinated membranes were measured. The voltage output of the RED stack slightly reduced for IEMs with greater hypochlorite exposure in 0-5000 ppm, as a result of the decreased membrane permselectivity (Fig. 9). The increased internal resistance of the RED stack (Fig. 11c), reflected by the slope of polarization curve, is consistent with the greater resistance of the IEMs after chlorination (section 3.2.2). The combined effects of reduced voltage and increased internal resistance caused a significant reduction in RED power density (Fig. 11b).

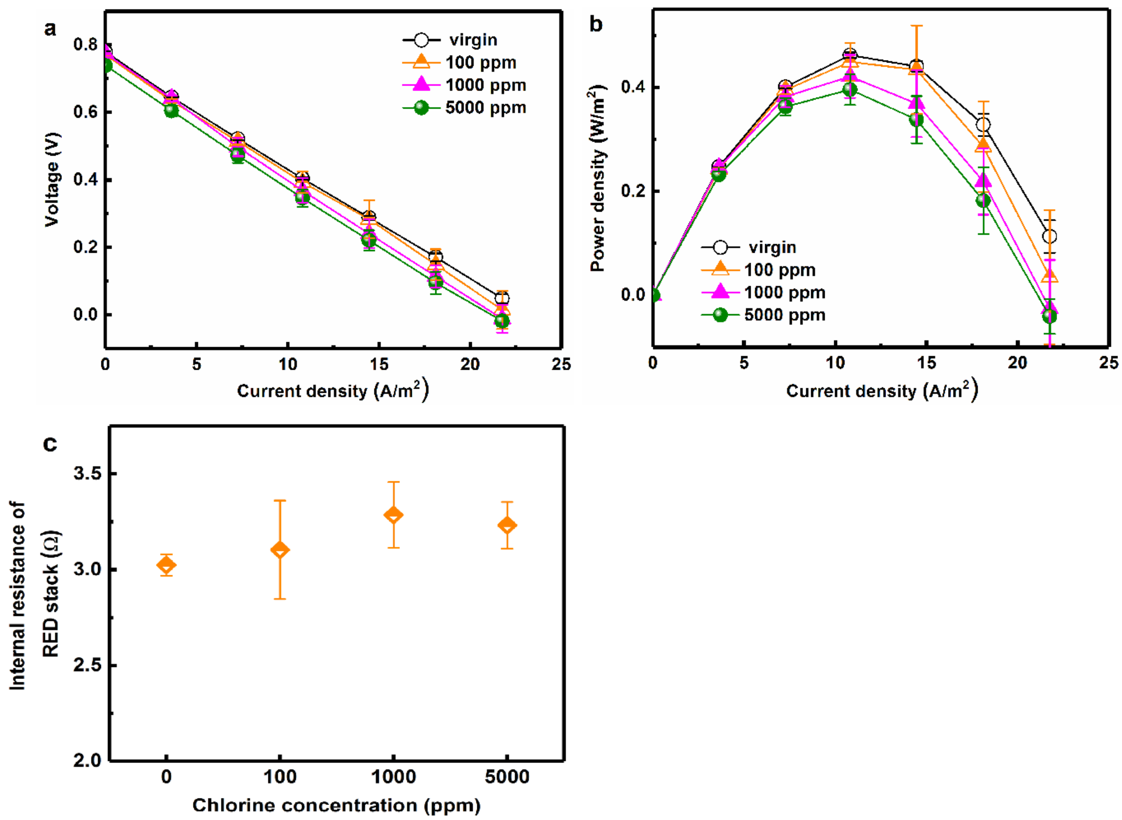

Fig. 11. The polarization curve (a), the power production (b) and the corresponding internal resistance (c) of an RED stack with IEMs chlorinated in 0 ppm, 100 ppm, 1000 ppm and 5000 ppm at pH 7 for 50 h. The feed solutions were synthetic 0.02 M NaCl and 0.6 M NaCl. The operation temperature was about 25 °C.

To further differentiate the roles of CEM chlorination vs. AEM chlorination, we included additional RED performance tests where only CEMs (or AEMs) were chlorinated (Fig. 12). Compared to the control case with no chlorination, exposure of CEMs to 5000 ppm hypochlorite had little influence on the RED power performance. In contrast, chlorination of AEMs under otherwise identical conditions reduced the power density from 0.46 W/m^2 to 0.39 W/m^2. Indeed, this reduced power density was nearly identical to that corresponding to the case where both CEMs and AEMs were chlorinated. The current results clearly suggest that the deteriorated power performance was mainly caused by AEM chlorination, which is also consistent with its lower chlorine resistance (Section 3.2.2). Thus, future studies shall focus the development of more chlorine-resistance AEM membranes.

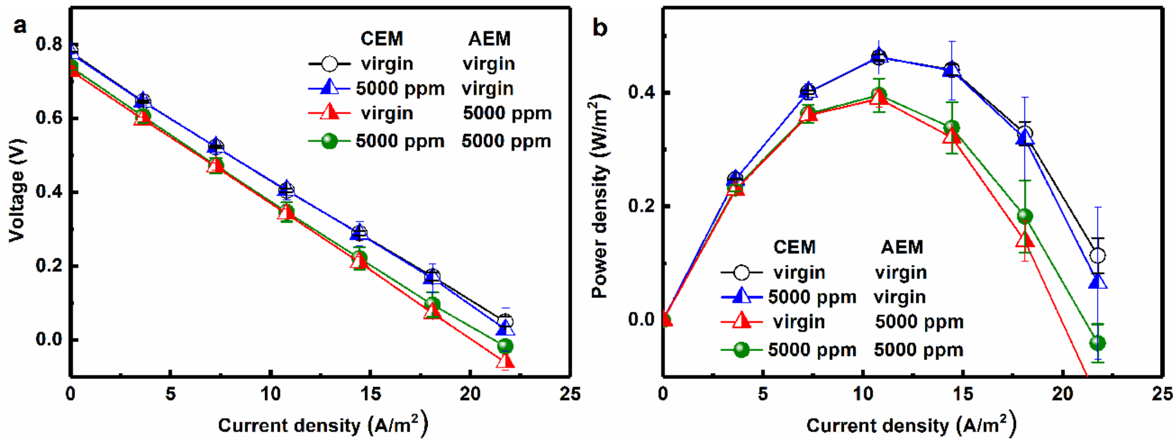

Fig. 12. The polarization curve (a) and the power production (b) of an RED stack with only CEMs or AEMs chlorinated in 5000 ppm at pH 7 for 50 h, virgin case with no chlorination and the case where both CEMs and AEMs chlorinated in 5000 ppm at pH 7 for 50 h. The feed solutions were synthetic 0.02 M NaCl and 0.6 M NaCl. The operation temperature was about 25 °C.

4. Conclusion

In this study, the effects of hypochlorite exposure and corresponding chlorination mechanisms were investigated for both CEMs and AEMs. The surface morphology of both types of membranes were significantly altered upon hypochlorite exposure, and IEC of the membranes were adversely impacted as a result of the cleavage of $–SO_3^-$ containing fraction for CEMs or $–NR_3^+$ containing fraction for AEMs. Compared to the CEM, the AEM in the current study was more prone to chlorination. The extensive development of cracks in the latter membrane dramatically increased its electrical resistance and reduced FCD and permselectivity, especially under severe chlorination conditions (e.g., 5000 ppm hypochlorite exposure). Consistent with its weaker chlorine resistance, RED performance tests revealed the dominant role of AEM chlorination on the power output.

Acknowledgements

This work is supported by the Strategic Research Theme (Clean Energy) and the Seed Fund for Incubating Group-based Collaborative Research Projects – Collaborative Research Fund, both funded by the University of Hong Kong (HKU). We also thank for the partial support from the Seed Fund for Basic Research (201411159110) at the HKU.

References

[1] R. Pattle, Production of electric power by mixing fresh and salt water in the hydroelectric pile, Nature, 174 (1954).
[2] J.W. Post, J. Veerman, H.V.M. Hamelers, G.J.W. Euverink, S.J. Metz, K. Nymeijer, C.J.N. Buisman, Salinity-gradient power: Evaluation of pressure-retarded osmosis and reverse electrodialysis, Journal of Membrane Science, 288 (2007) 218-230.
[3] B.E. Logan, M. Elimelech, Membrane-based processes for sustainable power generation using water, Nature, 488 (2012) 313-319.
[4] N.Y. Yip, D.A. Vermaas, K. Nijmeijer, M. Elimelech, Thermodynamic, energy efficiency, and power density analysis of reverse electrodialysis power generation with natural salinity gradients, Environmental Science & Technology, (2014).
[5] N.Y. Yip, M. Elimelech, Comparison of energy efficiency and power density in pressure retarded osmosis and reverse electrodialysis, Environmental Science & Technology, 48 (2014) 11002-11012.
[6] M. Tedesco, A. Cipollina, A. Tamburini, G. Micale, Towards 1kW power production in a reverse electrodialysis pilot plant with saline waters and concentrated brines, Journal of Membrane Science, 522 (2017) 226-236.
[7] S. Ratkje, T. Holt, L. Fiksdal, Effect of biofilm formation on salinity power plant output on a laboratory scale, AIChE Symp. Ser, (1986) 39-44.
[8] D.A. Vermaas, D. Kunteng, M. Saakes, K. Nijmeijer, Fouling in reverse electrodialysis under natural conditions, Water research, 47 (2013) 1289-1298.
[9] H. Susanto, M. Fitrianingtyas, A.M. Samsudin, A. Syakur, Experimental study of the natural organic matters effect on the power generation of reverse electrodialysis, International Journal of Energy Research, (2017).
[10] D.A. Vermaas, D. Kunteng, J. Veerman, M. Saakes, K. Nijmeijer, Periodic feedwater reversal and air sparging as antifouling strategies in reverse electrodialysis, Environmental Science & Technology, 48 (2014) 3065-3073.
[11] Z. He, X. Gao, Y. Zhang, Y. Wang, J. Wang, Revised spacer design to improve hydrodynamics and anti-fouling behavior in reverse electrodialysis processes, Desalination and Water Treatment, 57 (2016) 28176-28186.
[12] M. Vaselbehagh, H. Karkhanechi, R. Takagi, H. Matsuyama, Biofouling phenomena on anion exchange membranes under the reverse electrodialysis process, Journal of Membrane Science, 530 (2017) 232-239.
[13] C.H. Wei, X. Huang, R. Ben Aim, K. Yamamoto, G. Amy, Critical flux and chemical cleaning-in-place during the long-term operation of a pilot-scale submerged membrane bioreactor for municipal wastewater treatment, Water Research, 45 (2011) 863-871.
[14] S. Rouaix, C. Causserand, P. Aimar, Experimental study of the effects of hypochlorite on polysulfone membrane properties, Journal of Membrane Science, 277 (2006) 137-147.
[15] V.T. Do, C.Y. Tang, M. Reinhard, J.O. Leckie, Effects of chlorine exposure conditions on

physiochemical properties and performance of a polyamide membrane--mechanisms and implications, Environmental Science & Technology, 46 (2012) 13184-13192.
[16] X. Tang, S. Flint, R. Bennett, J. Brooks, The efficacy of different cleaners and sanitisers in cleaning biofilms on UF membranes used in the dairy industry, Journal of Membrane Science, 352 (2010) 71-75.
[17] W. Garcia-Vasquez, R. Ghalloussi, L. Dammak, C. Larchet, V. Nikonenko, D. Grande, Structure and properties of heterogeneous and homogeneous ion-exchange membranes subjected to ageing in sodium hypochlorite, Journal of Membrane Science, 452 (2014) 104-116.
[18] Eaton, A. D.; Clesceri, L. S.; Greenberg, A. E.,, Standard methods for examination of water and wastewater, APHA, AWWA and WEF: Washington DC, 1995.
[19] V.T. Do, C.Y. Tang, M. Reinhard, J.O. Leckie, Degradation of polyamide nanofiltration and reverse osmosis membranes by hypochlorite, Environmental Science & Technology, 46 (2012) 852-859.
[20] V.T. Do, C.Y. Tang, M. Reinhard, J.O. Leckie, Effects of hypochlorous acid exposure on the rejection of salt, polyethylene glycols, boron and arsenic(V) by nanofiltration and reverse osmosis membranes, Water Research, 46 (2012) 5217-5223.
[21] A.H. Galama, D.A. Vermaas, J. Veerman, M. Saakes, H.H.M. Rijnaarts, J.W. Post, K. Nijmeijer, Membrane resistance: The effect of salinity gradients over a cation exchange membrane, Journal of Membrane Science, 467 (2014) 279-291.
[22] G.M. Geise, M.A. Hickner, B.E. Logan, Ionic resistance and permselectivity tradeoffs in anion exchange membranes, ACS Applied Materials & Interfaces, 5 (2013) 10294-10301.
[23] E. Güler, R. Elizen, D.A. Vermaas, M. Saakes, K. Nijmeijer, Performance-determining membrane properties in reverse electrodialysis, Journal of Membrane Science, 446 (2013) 266-276.
[24] P. Dlugolecki, K. Nymeijer, S. Metz, M. Wessling, Current status of ion exchange membranes for power generation from salinity gradients, Journal of Membrane Science, 319 (2008) 214-222.
[25] A.H. Galama, N.A. Hoog, D.R. Yntema, Method for determining ion exchange membrane resistance for electrodialysis systems, Desalination, 380 (2016) 1-11.
[26] P. Długołęcki, P. Ogonowski, S.J. Metz, M. Saakes, K. Nijmeijer, M. Wessling, On the resistances of membrane, diffusion boundary layer and double layer in ion exchange membrane transport, Journal of Membrane Science, 349 (2010) 369-379.
[27] J. Veerman, R.M. de Jong, M. Saakes, S.J. Metz, G.J. Harmsen, Reverse electrodialysis: Comparison of six commercial membrane pairs on the thermodynamic efficiency and power density, Journal of Membrane Science, 343 (2009) 7-15.
[28] J.W. Post, H.V. Hamelers, C.J. Buisman, Energy recovery from controlled mixing salt and fresh water with a reverse electrodialysis system, Environmental Science & Technology, 42 (2008) 5785-5790.
[29] A. Daniilidis, D.A. Vermaas, R. Herber, K. Nijmeijer, Experimentally obtainable energy

from mixing river water, seawater or brines with reverse electrodialysis, Renewable Energy, 64 (2014) 123-131.
[30] Y. Mei, C.Y. Tang, Co-locating reverse electrodialysis with reverse osmosis desalination: Synergies and implications, Journal of Membrane Science, (2017).
[31] J. Veerman, M. Saakes, S.J. Metz, G.J. Harmsen, Reverse electrodialysis: Performance of a stack with 50 cells on the mixing of sea and river water, Journal of Membrane Science, 327 (2009) 136-144.
[32] J. Hubert, C. Poleunis, A. Delcorte, P. Laha, J. Bossert, S. Lambeets, A. Ozkan, P. Bertrand, H. Terryn, F. Reniers, Plasma polymerization of C4Cl6 and C 2H2Cl4 at atmospheric pressure, Polymer (United Kingdom), 54 (2013) 4085-4092.
[33] Z. Yang, Y. Dai, S. Wang, H. Cheng, J. Yu, In situ incorporation of a S, N doped carbon/sulfur composite for lithium sulfur batteries, RSC Advances, 5 (2015) 78017-78025.
[34] L. Gu, T. Lu, M. Zhang, L. Tou, Y. Zhang, Efficient oxidative chlorination of aromatics on saturated sodium chloride solution, Advanced Synthesis and Catalysis, 355 (2013) 1077-1082.
[35] R. Lucena, S. Cárdenas, M. Gallego, M. Valcárcel, ATR-FTIR membrane-based sensor for the simultaneous determination of surfactant and oil total indices in industrial degreasing baths, Analyst, 131 (2006) 415-421.
[36] J.A. Vega, C. Chartier, W.E. Mustain, Effect of hydroxide and carbonate alkaline media on anion exchange membranes, Journal of Power Sources, 195 (2010) 7176-7180.
[37] T. Xu, J.-J. Woo, S.-J. Seo, S.-H. Moon, In situ polymerization: A novel route for thermally stable proton-conductive membranes, Journal of Membrane Science, 325 (2008) 209-216.
[38] H. Deng, Z. Wang, W. Zhang, B. Hu, S. Zhang, Preparation and monovalent selective properties of multilayer polyelectrolyte modified cation-exchange membranes, Journal of Applied Polymer Science, 132 (2015) n/a-n/a.
[39] H. Guo, L. Xiao, S. Yu, H. Yang, J. Hu, G. Liu, Y. Tang, Analysis of anion exchange membrane fouling mechanism caused by anion polyacrylamide in electrodialysis, Desalination, 346 (2014) 46-53.
[40] B.V. Bhut, S.R. Wickramasinghe, S.M. Husson, Preparation of high-capacity, weak anion-exchange membranes for protein separations using surface-initiated atom transfer radical polymerization, Journal of Membrane Science, 325 (2008) 176-183.
[41] J.V. Gulmine, P.R. Janissek, H.M. Heise, L. Akcelrud, Polyethylene characterization by FTIR, Polymer Testing, 21 (2002) 557-563.
[42] M. Beltran, A. Marcilla, Fourier transform infrared spectroscopy applied to the study of PVC decomposition, Eur Polym J, 33 (1997) 1135-1142.
[43] Z. Zhou, X. He, M. Zhou, F. Meng, Chemically induced alterations in the characteristics of fouling-causing bio-macromolecules - Implications for the chemical cleaning of fouled membranes, Water Research, 108 (2017) 115-123.
[44] J.-Y. Koo, R.J. Petersen, J.E. Cadotte, ESCA characterization of chlorine-damaged polyamide reverse osmosis membrane: American Chemical Society, Polymer Preprints,

Division of Polymer Chemistry, 1986, pp. 391-392.
[45] A. Simon, L.D. Nghiem, P. Le-Clech, S.J. Khan, J.E. Drewes, Effects of membrane degradation on the removal of pharmaceutically active compounds (PhACs) by NF/RO filtration processes, Journal of Membrane Science, 340 (2009) 16-25.